Micromorphic Homogenisation of a Porous Medium: Elastic Behavior and Quasi-brittle Damage

Article published in Continuum Mechanics and Thermodynamics. The final publication is available at www.springerlink.com, doi:10.1007/s00161-014-0402-5

Geralf Hütter, Uwe Mühlich, Meinhard Kuna

Today it is well-known that the classical Cauchy continuum theory is insufficient to describe the deformation behavior of solids if gradients occur over distances which are comparable to the microstructure of the material. This becomes crucial e.g. for small specimens or during localization of deformation induced by material degradation (damage). Higher order continuum approaches like micromorphic theories are established to address such problems. However, such theories require the formulation of respective constitutive laws, which account for the microstructural interactions. Especially in damage mechanics such laws are mostly formulated in a purely heuristic way, which leads to physical and numerical problems. In the present contribution the fully micromorphic constitutive law for a porous medium is obtained in closed form by homogenization based on the minimal boundary conditions concept. It is shown that this model describes size effects of porous media like foams adequately. The model is extended towards quasi-brittle damage overcoming the physical and numerical limitations of purely heuristic approaches.
keywords: size effects, homogenization, micromorphic theory, quasi-brittle damage

1 Introduction

Today, it is well-known that the mechanical response of porous materials like foams becomes dependent on the size of the used specimen if the dimension of the latter is comparable to the relevant microstructure length like the distance of pores or inclusions. If the behavior of structures made of such materials shall be simulated, the microstructure cannot be resolved everywhere in every detail. Rather, it is desirable to describe the material behavior in a smeared sense by means of a continuum theory. However, it is known that the classical Cauchy theory cannot describe the mentioned size effects. Merely, higher order continuum theories are necessary to model such effects. In the last years the micromorphic theory proposed first by Eringen and Suhubi [1] attracted research interest. In the micromorphic theory the current material state does not only depend on the macroscopic strain but additionally on the so-called microdeformation and its gradient. An overview over this theory will be given below. Due to this more detailed description of the microscopic state, size effects can be captured in principle.

However, this additional possibility necessitates the formulation of additional constitutive equations for the higher order stresses that arise as work-conjugate quantities to the additional deformation measures. This additional freedom means that already for an isotropic linear elastic material the number of independent constitutive parameters rises from two to 18 when going from the classical

Cauchy continuum to a fully micromorphic one. Of course, the experimental determination of this large number of parameters requires big efforts and the situation becomes even more severe if nonlinear material behavior is considered. Two different strategies have been pursued in literature to treat this problem. The first one is to use a reduced micromorphic theory like the micropolar one (also known as Cosserat theory). In this case the isotropic linear elastic material has six independent constitutive parameters, i.e. four additional ones. Determining four additional parameters from experimental [2–4] or numerical investigations [4–6] is typically seen as justifiable effort. However, it turned out the Cosserat theory does not recover all effects that are being observed with real materials. So this reduced theory has problems with the dispersion of longitudinal waves and with the size effects typically observed in bending specimens [2, 3, 7].

So recently, homogenization methods as proposed by Forest and Sab [8] attracted more attention to derive constitutive laws for micromorphic theories. However, due to the problem in treating fluctuation fields in this theory, the homogenizations were either done numerically [5, 9, 10] or restricted to constrained micromorphic theories where microdeformation and macrodeformation coincide a priori [11–15].

Damage mechanics is another field where classical Cauchy theory comes to its limits. Here, it is today well-established that classical theories are not able to describe the localization associated with softening adequately. For this reason advanced formulations accounting for additional gradient terms (besides the deformation gradient) like implicit gradient-enriched non-local models or phase-field models experience more and more popularity. According to Forest [16, 17] such formulations fit also in the (generalized) framework of micromorphic media. Referring to this framework the very most of the mentioned gradient-enriched damage models correspond to classical damage models extended heuristically by a linear and reversible constitutive relation between the additional gradient term and the respective conjugate stress-type quantity ("higher-order stress"). Such a linear and reversible constitutive relation is questionable in the context of the typically highly non-linear and dissipative constitutive relation for the classical Cauchy stress term and raises the problem of the interpretation of the respective coefficient(s). Furthermore, corresponding boundary conditions have to be specified for the higher order stresses. Typically, this is the trivial Neumann boundary condition for free surfaces. However, if the higher order stress is described by a linear and reversible constitutive law, it does not vanish in the fully damaged state. Thus, the fully damaged state does not correspond to the formation of a free surface [18], which is a counterintuitive prediction. For this reason it is highly desirable to obtain constitutive laws also for the higher order terms in a consistent way. Here, homogenization is a promising approach.

The intention of the present paper is to overcome the mentioned limitations and to derive a micromorphic constitutive model in closed form for porous media by homogenization. Based on these results a damage model is proposed.

The notation of the present contribution follows Forest and co-workers [see e.g. 19]. In particular scalars, vectors, second, third and forth order tensors are denoted by a, $\underline{\mathbf{b}}$, $\underset{\sim}{\mathbf{c}}$, $\underline{\underline{\mathbf{d}}}$ and $\underset{\approx}{\mathbf{e}}$, respectively. The operator $(\circ)^{\mathrm{T}}$ denotes the complete transposition of all indices of a tensor and $\mathrm{sym}\,(\circ)$ is the symmetric part of a second order tensor. Single to fourfold contractions are indicated by $\cdot$, $:$, $\vdots$, $::$, respectively, and are computed from left to right, i.e. $\underset{\approx}{\mathbf{e}} :: \underset{\approx}{\mathbf{f}} = e_{ijkl} f_{ijkl}$ using Einstein's summation rule over repeated indices and with e_{ijkl} referring to the coordinates of tensor $\underset{\approx}{\mathbf{e}}$ in a Cartesian system. The tensor product is written in a short notation as $\underline{\underline{\mathbf{ab}}}$. Only if the expressions maybe mistakable the symbol $\otimes$ is inserted equivalently as $\underline{\mathbf{a}} \otimes \underline{\mathbf{b}}$. Furthermore, ∇ denotes the nabla operator whose subscript denotes whether it is computed with respect to the macroscopic or the microscopic location vector.

2 Homogenisation for Micromorphic Continua

2.1 Macroscopic Deformation Measures

According to Germain [20], a homogenization of a continuum with microstructure can be performed by approximating the relevant microscopic field quantities, here the displacement, as

$$\tilde{\underline{\mathbf{u}}} = \underline{\mathbf{U}}(\underline{\mathbf{X}}) + \left(\underset{\sim}{\chi}(\underline{\mathbf{X}}) - \underset{\sim}{\mathbf{I}}\right) \cdot (\underline{\mathbf{x}} - \underline{\mathbf{X}}) \,. \tag{1}$$

The microscopic location vector is $\underline{\mathbf{x}}$ and $\underline{\mathbf{X}}$ refers to a macroscopic material point. Now the macroscopic displacement $\underline{\mathbf{U}}(\underline{\mathbf{X}})$ and the microdeformation $\underset{\sim}{\chi}(\underline{\mathbf{X}})$ are defined from the condition that the error between this approximation and the true microscopic field $\underline{\mathbf{u}}(\underline{\mathbf{x}})$ is minimized over a microstructural volume element $V(\underline{\mathbf{X}})$:

$$\left\langle \|\underline{\mathbf{u}}(\underline{\mathbf{x}}) - \tilde{\underline{\mathbf{u}}}\|^2 \right\rangle_{V(\underline{\mathbf{X}})} \xrightarrow{\underline{\mathbf{U}},\underset{\sim}{\chi}} \min. \tag{2}$$

whereby $\langle \circ \rangle_{V(\underline{\mathbf{X}})}$ means computing the average over $V(\underline{\mathbf{X}})$. If $\underline{\mathbf{X}}$ is now defined as the location of the geometric center of V, i.e. $\underline{\mathbf{X}} = \langle \underline{\mathbf{x}} \rangle_{V(\underline{\mathbf{X}})}$, then the optimization problem (2) yields [21]

$$\underline{\mathbf{U}}(\underline{\mathbf{X}}) = \langle \underline{\mathbf{u}} \rangle_{V(\underline{\mathbf{X}})} \tag{3}$$

$$\underset{\sim}{\chi}(\underline{\mathbf{X}}) = \underset{\sim}{\mathbf{I}} + \langle \underline{\mathbf{u}}(\underline{\mathbf{x}}) \otimes (\underline{\mathbf{x}} - \underline{\mathbf{X}}) \rangle_{V(\underline{\mathbf{X}})} \cdot \underset{\sim}{\mathbf{G}}^{-1} \tag{4}$$

with the second order geometrical moment tensor

$$\underset{\sim}{\mathbf{G}} = \langle (\underline{\mathbf{x}} - \underline{\mathbf{X}}) \otimes (\underline{\mathbf{x}} - \underline{\mathbf{X}}) \rangle_{V(\underline{\mathbf{X}})} \,. \tag{5}$$

As in classical continuum theory the macroscopic gradients of the primary macroscopic field variables $\underline{\mathbf{U}}(\underline{\mathbf{X}})$ and $\underset{\sim}{\chi}(\underline{\mathbf{X}})$ are introduced as deformation measures, that is the macroscopic deformation gradient $\underset{\sim}{\mathbf{F}} = \underset{\sim}{\mathbf{I}} + \underline{\mathbf{U}} \otimes \nabla_{\underline{\mathbf{X}}}$ and the higher order deformation gradient $\underset{\approx}{\mathbf{K}} = \underset{\sim}{\chi} \otimes \nabla_{\underline{\mathbf{X}}}$. Using definitions (3) and (4) it can be shown [see e.g. 21] that these quantities can be computed from the microscopic displacement field $\underline{\mathbf{u}}(\underline{\mathbf{x}})$ as

$$\underset{\sim}{\mathbf{F}} = \underset{\sim}{\mathbf{I}} + \left\langle \left(\nabla_{\underline{\mathbf{x}}} \underline{\mathbf{u}}\right)^{\mathrm{T}} \right\rangle_{V(\underline{\mathbf{X}})} \tag{6}$$

$$K_{ijk} = \left\langle \frac{\partial u_i}{\partial x_k} (x_m - X_m) \right\rangle_{V(\underline{\mathbf{X}})} G^{-1}_{mj} \tag{7}$$

For a homogeneous deformation $\underline{\mathbf{u}} = \hat{\underset{\sim}{\mathbf{F}}} \cdot \underline{\mathbf{x}} + \hat{\underline{\mathbf{u}}}$ with constants $\hat{\underset{\sim}{\mathbf{F}}}$ and $\hat{\underline{\mathbf{u}}}$ the aforementioned quantities are $\underset{\sim}{\mathbf{F}} = \underset{\sim}{\chi} = \hat{\underset{\sim}{\mathbf{F}}}$ and $\underset{\approx}{\mathbf{K}} = 0$. In the following only small strains are considered. Then, common deformation measures are the usual macroscopic strain $\underset{\sim}{\mathbf{E}} = 1/2(\underset{\sim}{\mathbf{F}} + \underset{\sim}{\mathbf{F}}^{\mathrm{T}}) - \underset{\sim}{\mathbf{I}}$, the difference between macroscopic deformation gradient and microdeformation $\underset{\sim}{\mathbf{e}} = \underset{\sim}{\mathbf{F}} - \underset{\sim}{\chi}$ and the microdeformation gradient $\underset{\approx}{\mathbf{K}}$.

2.2 Kinetics and minimal boundary conditions concept

According to the Hill-Mandel condition the macroscopic strain energy density is introduced as average of the corresponding microscopic quantity ψ over the microstructural volume element:

$$\Psi = \langle \psi \rangle_{V(\underline{\mathbf{X}})} \,. \tag{8}$$

It is well-known that, in contrast to the classical homogenization procedure, the particular values of the higher-order deformation measures $\underset{\sim}{\chi}$ and $\underset{\approx}{\mathbf{K}}$ according to definitions (4) and (7) cannot be converted

to surface integrals and can thus not be prescribed directly via displacement boundary conditions [22]. Merely, values of $\underset{\sim}{\underset{\sim}{\mathbf{K}}}$ and $\underset{\sim}{\chi}$ can be prescribed only as integral constraint over the whole domain of the microstructural volume element. Furthermore, in contrast to classical homogenization no periodic conditions can be derived. That is why Jänicke and Steeb [23] proposed in their "minimal boundary conditions concept" to implement only these integral type conditions but no other essential boundary conditions.

We consider now linear elastic material in the microstructural volume element under isothermal conditions. Thus, Eq. (8) becomes

$$\Psi = \left\langle \frac{1}{2}\underset{\sim}{\varepsilon} : \underset{\approx}{\mathbf{S}} : \underset{\sim}{\varepsilon} \right\rangle_{V(\underline{\mathbf{X}})} \tag{9}$$

with the local strain $\underset{\sim}{\varepsilon}(\underline{\mathbf{x}}) = 1/2[\nabla_{\underline{\mathbf{x}}}\tilde{\underline{\mathbf{u}}} + \left(\nabla_{\underline{\mathbf{x}}}\tilde{\underline{\mathbf{u}}}\right)^{\mathrm{T}}]$ for any local displacement field $\tilde{\underline{\mathbf{u}}}(\underline{\mathbf{x}})$. Therein, $\underset{\approx}{\mathbf{S}}$ denotes the local stiffness tensor.

According to the minimal boundary conditions concept, the actual microscopic displacement field $\underline{\mathbf{u}}(\underline{\mathbf{x}})$ is now the one which minimizes the macroscopic strain energy

$$\Psi = \min_{\underline{\mathbf{u}}(\underline{\mathbf{x}})} \left\langle \frac{1}{2}\nabla_{\underline{\mathbf{x}}}\underline{\mathbf{u}} : \underset{\approx}{\mathbf{S}} : \nabla_{\underline{\mathbf{x}}}\underline{\mathbf{u}} \right\rangle_{V(\underline{\mathbf{X}})} \qquad \text{under constraints (3), (4), (6) and (7)} \tag{10}$$

for prescribed values of the macroscopic quantities $\{\underline{\mathbf{U}}, \underset{\sim}{\chi}, \underset{\sim}{\mathbf{F}}, \underset{\sim}{\underset{\sim}{\mathbf{K}}}\}$ or, equivalently, $\{\underline{\mathbf{U}}, \underset{\sim}{\mathbf{E}}, \underset{\sim}{\mathbf{e}}, \underset{\sim}{\underset{\sim}{\mathbf{K}}}\}$. Of course, it will turn out that Ψ does not depend explicitly on the macroscopic displacement $\underline{\mathbf{U}}$ due to objectivity of the continuum theory on the microscopic level. In Eq. (10) the left and right sub symmetry of the stiffness tensor $\underset{\approx}{\mathbf{S}}$ was used to symmetrize the displacement gradient $\nabla_{\underline{\mathbf{x}}}\underline{\mathbf{u}}$. The stresses that are work-conjugate to the deformation measures are then obtained as

$$\underset{\sim}{\mathbf{s}} = \frac{\partial \Psi}{\partial \underset{\sim}{\mathbf{e}}}, \qquad \underset{\sim}{\mathbf{\Sigma}} = \frac{\partial \Psi}{\partial \underset{\sim}{\mathbf{E}}}, \qquad \underset{\sim}{\underset{\sim}{\mathbf{M}}} = \frac{\partial \Psi}{\partial \underset{\sim}{\underset{\sim}{\mathbf{K}}}} \tag{11}$$

and fulfill (in absence of inertia and volume forces) the balance equations

$$\left(\underset{\sim}{\mathbf{\Sigma}} + \underset{\sim}{\mathbf{s}}\right) \cdot \nabla_{\underline{\mathbf{X}}} = 0 \tag{12}$$

$$\underset{\sim}{\mathbf{s}} + \underset{\sim}{\underset{\sim}{\mathbf{M}}} \cdot \nabla_{\underline{\mathbf{X}}} = 0\,, \tag{13}$$

see e.g. [19, 20].

2.3 Local Displacement Field

This variational problem (10) is solved in the present study approximately by Ritz' method. Facing the large number of kinematic constraints, a polynomial ansatz

$$\underline{\mathbf{u}}(\underline{\mathbf{x}}) = \underline{\mathbf{A}} + \underset{\sim}{\mathbf{B}} \cdot \underline{\mathbf{x}} + \frac{1}{2}\underset{\sim}{\underset{\sim}{\mathbf{C}}} : \underline{\mathbf{xx}} + \frac{1}{3}\underset{\approx}{\mathbf{D}} \vdots \underline{\mathbf{xxx}} \tag{14}$$

is employed for the microscopic displacement field as established in literature on micromorphic homogenisation [5, 8, 9, 21, 22, 24]. Here $\underline{\mathbf{X}} = 0$ is assumed without loss of generality. The polynomial tensors $\underline{\mathbf{xx}}$ and $\underline{\mathbf{xxx}}$ are completely symmetric and so are the coefficient tensors $\underset{\sim}{\underset{\sim}{\mathbf{C}}}$ and $\underset{\approx}{\mathbf{D}}$ with respect to the corresponding indices.

Inserting this field in the mentioned definitions (4), (6), (7) and respecting the symmetry properties of the tensors yields (for a centrosymmetric unit cell, i.e. $\langle \underline{\mathbf{x}}^n \rangle_{V(\underline{\mathbf{X}})} = 0$ for odd n) :

$$\underset{\sim}{\mathbf{F}} = \underset{\sim}{\mathbf{I}} + \underset{\sim}{\mathbf{B}} + \underset{\approx}{\mathbf{D}} : \underset{\sim}{\mathbf{G}} \tag{15}$$

$$\underset{\sim}{\chi} = \underset{\sim}{\mathbf{I}} + \underset{\sim}{\mathbf{B}} + \frac{1}{3}\underset{\approx}{\mathbf{D}} \vdots \underset{\approx}{\mathbf{G}}^4 \cdot \underset{\sim}{\mathbf{G}}^{-1} \tag{16}$$

$$\underset{\sim}{\underset{\sim}{\mathbf{K}}} = \underset{\sim}{\underset{\sim}{\mathbf{C}}} \tag{17}$$

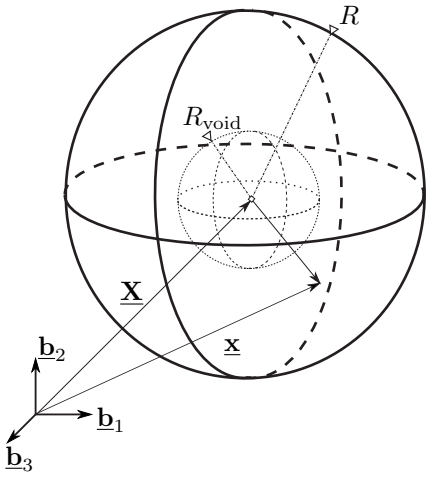

Figure 1: Spherical microstructural volume element with void (from [26])

Therein, $\underset{\sim}{\mathbf{G}} = \langle \underline{\mathbf{x}}\underline{\mathbf{x}} \rangle_{V(\underline{\mathbf{X}})}$ and $\underset{\approx}{\mathbf{G}}^4 = \langle \underline{\mathbf{x}}\underline{\mathbf{x}}\underline{\mathbf{x}}\underline{\mathbf{x}} \rangle_{V(\underline{\mathbf{X}})}$ are the second and forth order geometrical moments. The corresponding constitutive strain-like deformation measures are obtained as

$$\begin{aligned} \underset{\sim}{\mathbf{E}} &= \operatorname{sym}\left(\underset{\sim}{\mathbf{B}}\right) + \operatorname{sym}\left(\underset{\approx}{\mathbf{D}} : \underset{\sim}{\mathbf{G}}\right) \\ \underset{\sim}{\mathbf{e}} &= \underset{\approx}{\mathbf{D}} \vdots \left(\underset{\sim}{\mathbf{G}}\underset{\sim}{\mathbf{I}} - \frac{1}{3}\underset{\approx}{\mathbf{G}}^4 \cdot \underset{\sim}{\mathbf{G}}^{-1}\right) \\ \underset{\sim\sim}{\mathbf{K}} &= \underset{\sim\sim}{\mathbf{C}}\,. \end{aligned} \tag{18}$$

At first glance it may look as if the coefficient tensors $\underset{\sim}{\mathbf{B}}$, $\underset{\sim\sim}{\mathbf{C}}$ and $\underset{\approx}{\mathbf{D}}$ were directly tied by Eqs. (18) for given set of macroscopic deformations $\underset{\sim}{\mathbf{E}}$, $\underset{\sim}{\mathbf{e}}$ and $\underset{\sim\sim}{\mathbf{K}}$. However, the coefficient tensor $\underset{\approx}{\mathbf{D}}$ of the cubic part of the polynomial has 30 independent components whereas $\underset{\sim}{\mathbf{e}}$ has only nine [22, 25]. Thus, $\underset{\approx}{\mathbf{D}}$ is not defined uniquely by the microstrain difference tensor $\underset{\sim}{\mathbf{e}}$ but further assumptions are necessary. In contrast, the third order polynomial tensor $\underset{\sim\sim}{\mathbf{C}}$ is sub-symmetric with respect to the right indices whereas definition (7) does not imply this property a priori for $\underset{\sim\sim}{\mathbf{K}}$. In the cited references [5, 8, 9, 21, 22, 24] the cubic coefficient tensor $\underset{\approx}{\mathbf{D}}$ was filled more or less arbitrarily with components of the microdeformation difference tensor $\underset{\sim}{\mathbf{e}}$ to fulfill Eq. (18). In the aforementioned studies the polynomial displacement field (14) determined this way is prescribed either in the whole domain of the microstructural volume element or only at its boundary. In the latter case the definitions (4),(6),(7) of the macroscopic quantities $\underset{\sim}{\mathbf{F}}$, $\underset{\sim}{\chi}$, $\underset{\sim\sim}{\mathbf{K}}$ and consequently of $\underset{\sim}{\mathbf{E}}$, $\underset{\sim}{\mathbf{e}}$ and $\underset{\sim\sim}{\mathbf{K}}$ are violated in general [22]. With the present approach of formulating the boundary value problem (in variational form (10)) under strict enforcement of (4),(6) and (7) both problems do not appear and the local displacement field and the associated energy can be determined with consistent kinematics and with arbitrary accuracy, e.g. by taking higher order polynomials than (14) as ansatz and determining the additional coefficients of arbitrary number straight forward by Ritz' method.

3 Spherical Microstructural Volume Element

The method is applied to a spherical microstructural volume element as sketched in Figure 1. For a spherical unit cell of radius R the geometrical moments are [26]

$$\underset{\sim}{\mathbf{G}} = \frac{1}{5}R^2\underset{\sim}{\mathbf{I}}, \qquad \underset{\approx}{\mathbf{G}}^4 = \frac{1}{35}R^4\left(2\underset{\approx}{\mathbf{I}}^{\mathrm{s}} + \underset{\sim\sim}{\mathbf{II}}\right) \tag{19}$$

wherein $\underset{\approx}{\mathbf{I}}^{\mathrm{s}}$ is the symmetrizing forth order unit tensor. Thus, (18) gives[1]

$$\underset{\sim}{\mathbf{e}} = \frac{2}{35} R^2 \underset{\approx}{\mathbf{D}} : \underset{\sim}{\mathbf{I}} \tag{20}$$

$$\underset{\sim}{\mathbf{E}} = \mathrm{sym}\left(\underset{\sim}{\mathbf{B}}\right) + \frac{7}{2}\mathrm{sym}\left(\underset{\sim}{\mathbf{e}}\right) . \tag{21}$$

Regarding the strain energy of this configuration it is clear that the void does not contribute due to its vanishing stiffness but only the matrix does. For this purpose the operator $\langle\circ\rangle_{\mathrm{M}} = 1/V \int_{V_{\mathrm{M}}} \circ \,\mathrm{d}V$ is defined that computes that integral over the matrix volume V_{M} (i.e. for $r = R_{\mathrm{void}} \ldots R$) divided by the total volume $V = V_{\mathrm{M}}/(1-f)$ of the RVE. Therein, f denotes the void volume fraction. Inserting the polynomial displacement field (14) into Eq. (10) thus yields a macroscopic strain energy density

$$\Psi = \left\langle \frac{1}{2}\left(\underset{\sim}{\mathbf{B}} + \underset{\sim\sim}{\mathbf{C}} \cdot \underline{\mathbf{x}} + \underset{\approx}{\mathbf{D}} : \underline{\underline{\mathbf{xx}}}\right) : \underset{\approx}{\mathbf{S}} : \left(\underset{\sim}{\mathbf{B}} + \underset{\sim\sim}{\mathbf{C}} \cdot \underline{\mathbf{x}} + \underset{\approx}{\mathbf{D}} : \underline{\underline{\mathbf{xx}}}\right) \right\rangle_{\mathrm{M}} \tag{22}$$

to be minimized. Expanding this expression and taking into account the central symmetry of the geometry leads to

$$\Psi = \frac{1}{2}\langle 1\rangle_{\mathrm{M}} \underset{\sim}{\mathbf{B}} : \underset{\approx}{\mathbf{S}} : \underset{\sim}{\mathbf{B}} + \frac{1}{2}\left(\underset{\sim\sim}{\mathbf{C}}^{\mathrm{T}} : \underset{\approx}{\mathbf{S}} : \underset{\sim\sim}{\mathbf{C}}\right) : \langle \underline{\underline{\mathbf{xx}}}\rangle_{\mathrm{M}} + \frac{1}{2}\left(\underset{\approx}{\mathbf{D}}^{\mathrm{T}} : \underset{\approx}{\mathbf{S}} : \underset{\approx}{\mathbf{D}}\right) :: \langle \underline{\underline{\underline{\underline{\mathbf{xxxx}}}}}\rangle_{\mathrm{M}} + \left(\underset{\sim}{\mathbf{B}}^{\mathrm{T}} : \underset{\approx}{\mathbf{S}} : \underset{\approx}{\mathbf{D}}\right) : \langle \underline{\underline{\mathbf{xx}}}\rangle_{\mathrm{M}} . \tag{23}$$

where it was assumed that the stiffness tensor $\underset{\approx}{\mathbf{S}}$ does not depend on microscopic location $\underline{\mathbf{x}}$. The weighted integrals over the hollow sphere evaluate to

$$\langle 1\rangle_{\mathrm{M}} = 1 - f \qquad \langle \underline{\underline{\mathbf{xx}}}\rangle_{\mathrm{M}} = \left(1 - f^{5/3}\right)\frac{R^2}{5}\underset{\sim}{\mathbf{I}} \qquad \langle \underline{\underline{\underline{\underline{\mathbf{xxxx}}}}}\rangle_{\mathrm{M}} = \left(1 - f^{7/3}\right)\frac{R^4}{35}\left(2\underset{\approx}{\mathbf{I}}^{\mathrm{s}} + \underset{\sim\sim}{\mathbf{II}}\right) . \tag{24}$$

Now the coefficient tensors $\underset{\sim}{\mathbf{B}}$, $\underset{\sim\sim}{\mathbf{C}}$ and $\underset{\approx}{\mathbf{D}}$ have to be substituted by the macroscopic deformation measures $\underset{\sim}{\mathbf{E}}$, $\underset{\sim\sim}{\mathbf{K}}$ and $\underset{\sim}{\mathbf{e}}$ from (18). In (23) the first two terms on the right-hand side can be evaluated immediately by means of (18) and (21). Also the mixed term $\left(\underset{\sim}{\mathbf{B}}^{\mathrm{T}} : \underset{\approx}{\mathbf{S}} : \underset{\approx}{\mathbf{D}}\right) : \langle \underline{\underline{\mathbf{xx}}}\rangle_{\mathrm{M}}$ can be evaluated directly since $\langle \underline{\underline{\mathbf{xx}}}\rangle_{\mathrm{M}}$ is spherical according to Eq. (24) and $\underset{\approx}{\mathbf{D}} : \underset{\sim}{\mathbf{I}}$ can be substituted by $\underset{\sim}{\mathbf{e}}$ according to Eq. (20). The quadratic term in $\underset{\approx}{\mathbf{D}}$ goes with $\langle \underline{\underline{\underline{\underline{\mathbf{xxxx}}}}}\rangle_{\mathrm{M}}$. The latter is a linear combination of $\underset{\sim\sim}{\mathbf{II}}$ and $\underset{\approx}{\mathbf{I}}^{\mathrm{s}}$. The former part $\underset{\sim\sim}{\mathbf{II}}$ results in terms $\left(\underset{\approx}{\mathbf{D}}^{\mathrm{T}} : \underset{\approx}{\mathbf{S}} : \underset{\approx}{\mathbf{D}}\right) :: \underset{\sim\sim}{\mathbf{II}} = (\underset{\approx}{\mathbf{D}} : \underset{\sim}{\mathbf{I}}) : \underset{\approx}{\mathbf{S}} : (\underset{\approx}{\mathbf{D}} : \underset{\sim}{\mathbf{I}})$ that can again be evaluated directly to $\underset{\sim}{\mathbf{e}}$ according to (20). Thus, one obtains in a first step

$$\begin{aligned}\Psi = {} & \frac{1}{2}(1-f)\left(\underset{\sim}{\mathbf{E}} - \frac{7}{2}\underset{\sim}{\mathbf{e}}\right) : \underset{\approx}{\mathbf{S}} : \left(\underset{\sim}{\mathbf{E}} - \frac{7}{2}\underset{\sim}{\mathbf{e}}\right) + \frac{R^2}{10}\left(1 - f^{5/3}\right)\left(\underset{\sim\sim}{\mathbf{K}}^{\mathrm{T}} : \underset{\approx}{\mathbf{S}} : \underset{\sim\sim}{\mathbf{K}}\right) : \underset{\sim}{\mathbf{I}} \\ & + \left(1 - f^{7/3}\right)\frac{R^4}{70}\left(\frac{35}{9R^2}\underset{\sim}{\mathbf{e}}\right) : \underset{\approx}{\mathbf{S}} : \left(\frac{35}{9R^2}\underset{\sim}{\mathbf{e}}\right) + \left(1 - f^{7/3}\right)\frac{R^4}{35}\left(\underset{\approx}{\mathbf{D}} : \underset{\approx}{\mathbf{I}}^{\mathrm{s}} : \underset{\approx}{\mathbf{D}}^{\mathrm{T}}\right) :: \underset{\approx}{\mathbf{S}} \\ & + \left(1 - f^{5/3}\right)\frac{R^2}{5}\left(\underset{\sim}{\mathbf{E}} - \frac{7}{2}\underset{\sim}{\mathbf{e}}\right) : \underset{\approx}{\mathbf{S}} : \left(\frac{35}{9R^2}\underset{\sim}{\mathbf{e}}\right)\end{aligned} \tag{25}$$

Collecting some terms results in

$$\begin{aligned}\Psi = {} & \frac{1}{2}(1-f)\underset{\sim}{\mathbf{E}} : \underset{\approx}{\mathbf{S}} : \underset{\sim}{\mathbf{E}} + \frac{R^2}{2}F^K(f)\left(\underset{\sim\sim}{\mathbf{K}}^{\mathrm{T}} : \underset{\approx}{\mathbf{S}} : \underset{\sim\sim}{\mathbf{K}}\right) : \underset{\sim}{\mathbf{I}} + F^{Ee}(f)\underset{\sim}{\mathbf{E}} : \underset{\approx}{\mathbf{S}} : \underset{\sim}{\mathbf{e}} \\ & - \frac{7}{8}\left(2 + 7f - 14f^{5/3} + 5f^{7/3}\right)\underset{\sim}{\mathbf{e}} : \underset{\approx}{\mathbf{S}} : \underset{\sim}{\mathbf{e}} + \left(1 - f^{7/3}\right)\frac{R^4}{35}\left(\underset{\approx}{\mathbf{D}} : \underset{\approx}{\mathbf{I}}^{\mathrm{s}} : \underset{\approx}{\mathbf{D}}^{\mathrm{T}}\right) :: \underset{\approx}{\mathbf{S}} .\end{aligned} \tag{26}$$

[1] Employing Eq. (18) to the microstructural volume element with void to obtain Eqs. $(18)_3$ and (20) means that the displacement field is defined also in the void, i.e. it corresponds to the limit case of elastic material in the void but with vanishing stiffness. This assumption is necessary since, as mentioned already, (4) and (7) cannot be converted to surface integrals.

The coefficient functions $F^K(f)$ and $F^{Ee}(f)$ will be summarized below. The last term $\underset{\approx}{\mathbf{D}} : \underset{\approx}{\mathbf{I}}^{\mathrm{s}} : \underset{\approx}{\mathbf{D}}^{\mathrm{T}}$ in Eq. (26) cannot be expressed uniquely in terms of the macroscopic deformations $\underset{\sim}{\mathbf{E}}$, $\underset{\sim}{\underset{\sim}{\mathbf{K}}}$ and $\underset{\sim}{\mathbf{e}}$ but it contains a fluctuation field. According to the minimal boundary conditions concept the fluctuation field minimizes the total strain energy for given $\underset{\sim}{\mathbf{E}}$, $\underset{\sim}{\underset{\sim}{\mathbf{K}}}$ and $\underset{\sim}{\mathbf{e}}$. In Eq. (26) only $\underset{\approx}{\mathbf{D}}$ remains to be determined under constraint Eq. (20). The Lagrangian of the corresponding minimization problem reads

$$\mathcal{L} = \Psi_0\left(\underset{\sim}{\mathbf{E}}, \underset{\sim}{\underset{\sim}{\mathbf{K}}}, \underset{\sim}{\mathbf{e}}\right) + \left(1 - f^{7/3}\right) \frac{R^4}{35} \left(\underset{\approx}{\mathbf{D}} : \underset{\approx}{\mathbf{I}}^{\mathrm{s}} : \underset{\approx}{\mathbf{D}}^{\mathrm{T}}\right) :: \underset{\approx}{\mathbf{S}} + \underset{\sim}{\lambda} : \left(\underset{\sim}{\mathbf{e}} - \frac{2}{35} R^2 \underset{\approx}{\mathbf{D}} : \underset{\sim}{\mathbf{I}}\right) \tag{27}$$

and is to be minimized with respect to the polynomial coefficient tensor $\underset{\approx}{\mathbf{D}}$ and the Lagrange multiplier[2] $\underset{\sim}{\lambda}$. Therein, $\Psi_0(\underset{\sim}{\mathbf{E}}, \underset{\sim}{\underset{\sim}{\mathbf{K}}}, \underset{\sim}{\mathbf{e}})$ was introduced as a abbreviation for all terms in Eq. (26) that depend on the macroscopic deformations only. The stationarity conditions $\mathcal{L}_{,\underset{\sim}{\lambda}} = \underset{\sim}{\mathbf{0}}$ and $\mathcal{L}_{,\underset{\approx}{\mathbf{D}}} = \underset{\approx}{\mathbf{0}}$ give Eq. (20) and

$$\underset{\approx}{\mathbf{0}} = \left(1 - f^{7/3}\right) \frac{2R^4}{35} \underset{\approx}{\mathbf{S}} : \underset{\approx}{\mathbf{D}} - \frac{2}{35} R^2 \underset{\sim}{\lambda} \underset{\sim}{\mathbf{I}}. \tag{28}$$

Lagrange multiplier $\underset{\sim}{\lambda}$ can be determined by taking the (right) spherical part of (28) and inserting Eq. (20) yielding $\underset{\sim}{\lambda} = \left(1 - f^{7/3}\right) 35/6 \underset{\approx}{\mathbf{S}} : \underset{\sim}{\mathbf{e}}$. Inserting this value back into Eq. (28) gives

$$\underset{\approx}{\mathbf{S}} : \left(\underset{\approx}{\mathbf{D}} - \frac{35}{6R^2} \underset{\sim}{\mathbf{e}} \underset{\sim}{\mathbf{I}}\right) = \underset{\approx}{\mathbf{0}}. \tag{29}$$

Note that this does not imply that the bracketed term in Eq. (29) is zero but only its left symmetrized part. Thus, one obtains the left symmetrized part (by multiplying the compliance tensor from left) as

$$\underset{\approx}{\mathbf{I}}^{\mathrm{s}} : \underset{\approx}{\mathbf{D}} = \frac{35}{6R^2} \mathrm{sym}\left(\underset{\sim}{\mathbf{e}}\right) \underset{\sim}{\mathbf{I}}. \tag{30}$$

Only the latter is needed for computing the strain energy and inserting it back into Eq. (26) leads to the final result

$$\Psi = \frac{1}{2}(1-f) \underset{\sim}{\mathbf{E}} : \underset{\approx}{\mathbf{S}} : \underset{\sim}{\mathbf{E}} + \frac{R^2}{2} F^K(f) \left(\underset{\sim}{\underset{\sim}{\mathbf{K}}}^{\mathrm{T}} : \underset{\approx}{\mathbf{S}} : \underset{\sim}{\underset{\sim}{\mathbf{K}}}\right) : \underset{\sim}{\mathbf{I}} + \frac{1}{2} F^{ee}(f) \underset{\sim}{\mathbf{e}} : \underset{\approx}{\mathbf{S}} : \underset{\sim}{\mathbf{e}} + F^{Ee}(f) \underset{\sim}{\mathbf{E}} : \underset{\approx}{\mathbf{S}} : \underset{\sim}{\mathbf{e}}. \tag{31}$$

The prefactors depend on the void volume fraction f and read

$$\begin{aligned} F^{ee}(f) &= \frac{7}{12}\left[4 - 21f + 42f^{5/3} - 25f^{7/3}\right] \\ F^{Ee}(f) &= \frac{7}{2} f \left(1 - f^{2/3}\right) \\ F^K(f) &= \frac{1}{5}\left(1 - f^{5/3}\right). \end{aligned} \tag{32}$$

They are plotted against f in Figure 2. The stresses are obtained from (31) according to (11) as

$$\underset{\sim}{\mathbf{s}} = \frac{\partial \Psi}{\partial \underset{\sim}{\mathbf{e}}} = F^{ee}(f) \underset{\approx}{\mathbf{S}} : \underset{\sim}{\mathbf{e}} + F^{Ee}(f) \underset{\approx}{\mathbf{S}} : \underset{\sim}{\mathbf{E}} \tag{33}$$

$$\underset{\sim}{\mathbf{\Sigma}} = \frac{\partial \Psi}{\partial \underset{\sim}{\mathbf{E}}} = (1-f) \underset{\approx}{\mathbf{S}} : \underset{\sim}{\mathbf{E}} + F^{Ee}(f) \underset{\approx}{\mathbf{S}} : \underset{\sim}{\mathbf{e}} \tag{34}$$

$$\underset{\sim}{\underset{\sim}{\mathbf{M}}} = \frac{\partial \Psi}{\partial \underset{\sim}{\underset{\sim}{\mathbf{K}}}} = R^2 F^K(f) \underset{\approx}{\mathbf{S}} : \underset{\sim}{\underset{\sim}{\mathbf{K}}} \tag{35}$$

[2] Actually, the assumed symmetry of $\underset{\approx}{\mathbf{D}}$ with respect to its right indices has to be enforced by a further Lagrange multiplier. However, this more lengthy procedure gives finally the same result Eq. (30) and is thus omitted here for the sake of clarity.

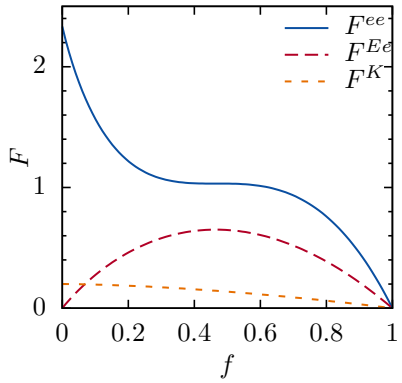

Figure 2: Prefactors as function of void volume fraction f

Note that the strain energy Ψ depends on the symmetric part of the difference strain $\underset{\sim}{\mathbf{e}}$ only since $\underset{\sim}{\mathbf{e}}$ appears in products with the symmetric stiffness tensor $\underset{\approx}{\mathbf{S}}$ only. Correspondingly, the conjugate stress $\underset{\sim}{\mathbf{s}}$ is symmetric. Also the higher-order stress $\underset{\approx}{\underset{\sim}{\mathbf{M}}}$ has a left sub-symmetry. Consequently, only six of the nine equations (13) are independent. Thus, in the classification of Forest and Sievert [19] the derived model describes a microstrain continuum.

4 Circular Microstructural Volume Element

The procedure can be applied analogously to a plane problem, i.e. to a circular microstructural volume element of radius R with circular void of R_{void}. Then f describes the void area fraction or, equivalently, the volume fraction of infinitely long cylindrical voids aligned normal to the loading plane. The geometrical moments are then

$$\underset{\sim}{\mathbf{G}} = \frac{1}{4}R^2\underset{\sim}{\mathbf{I}}, \qquad \underset{\approx}{\mathbf{G}}^4 = \frac{1}{24}R^4\left(2\underset{\approx}{\mathbf{I}}^{\text{s}} + \underset{\approx}{\underset{\sim}{\mathbf{II}}}\right) . \tag{36}$$

Now the second and forth order unit tensors $\underset{\sim}{\mathbf{I}}$ and $\underset{\approx}{\mathbf{I}}^{\text{s}}$ refer to their 2D analogs. Analogous to Eqs. (20) and (21) one obtains the relation between polynomial coefficients and deformation measures as

$$\underset{\sim}{\mathbf{e}} = \frac{R^2}{12}\underset{\approx}{\mathbf{D}} : \underset{\sim}{\mathbf{I}} \tag{37}$$

$$\underset{\sim}{\mathbf{E}} = \text{sym}\left(\underset{\sim}{\mathbf{B}}\right) + 3\text{sym}\left(\underset{\sim}{\mathbf{e}}\right) . \tag{38}$$

The procedure from the preceding section remains the same but with (24) replaced by

$$\langle 1\rangle_{\text{M}} = 1 - f \qquad \langle \underline{\mathbf{xx}}\rangle_{\text{M}} = \left(1 - f^2\right)\frac{R^2}{4}\underset{\sim}{\mathbf{I}} \qquad \langle \underline{\mathbf{xxxx}}\rangle_{\text{M}} = \left(1 - f^3\right)\frac{R^4}{24}\left(2\underset{\approx}{\mathbf{I}}^{\text{s}} + \underset{\approx}{\underset{\sim}{\mathbf{II}}}\right) . \tag{39}$$

Finally, also the resulting energy Eq. (31) and the derived stresses Eqs. 33 to (35) remain but with the prefactors

$$\begin{aligned} F^{ee}(f) &= 3\left[1 - 3f + 6f^2 - 4f^3\right] \\ F^{Ee}(f) &= 3f\left(1 - f\right) \\ F^{K}(f) &= \frac{1}{4}\left(1 - f^2\right) . \end{aligned} \tag{40}$$

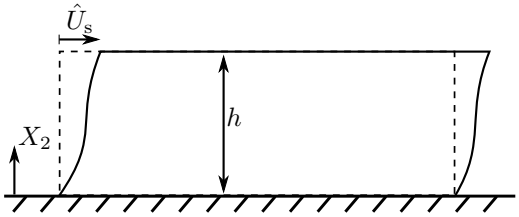

Figure 3: Simple shearing of an infinitely wide layer

5 Application

5.1 Size Effect in Simple Shear

In order to investigate the predictions of the presented model, the simple shearing of an infinitely wide layer of height h of the homogenized micromorphic material is considered as sketched in Figure 3. This one-dimensional problem can be solved analytically which is why it is often used as a benchmark to study size effects predicted by higher order continuum theories, e.g. in [6, 27–30]. For the present model (both spherical or circular voids) the kinematic quantities are given for the simple shear problem as

$$\underline{\mathbf{U}} = U_\mathrm{s}\left(X_2\right)\underline{\mathbf{b}}_1 \tag{41}$$

$$\underset{\sim}{\chi} = \chi_\mathrm{s}\left(X_2\right)\underline{\mathbf{b}}_1\underline{\mathbf{b}}_2 \tag{42}$$

with $\underline{\mathbf{b}}_1$ and $\underline{\mathbf{b}}_2$ denoting the unit base vectors. Then the strains are obtained as

$$\underset{\sim}{\mathbf{K}} = \chi_\mathrm{s}'\left(X_2\right)\underline{\mathbf{b}}_1\underline{\mathbf{b}}_2\underline{\mathbf{b}}_2 \tag{43}$$

$$\underset{\sim}{\mathbf{E}} = U_\mathrm{s}'\underset{\sim}{\mathbf{N}}_\mathrm{s} \tag{44}$$

$$\mathrm{sym}\left(\underset{\sim}{\mathbf{e}}\right) = \left(U_\mathrm{s}' - \chi_\mathrm{s}\right)\underset{\sim}{\mathbf{N}}_\mathrm{s} \tag{45}$$

wherein $\underset{\sim}{\mathbf{N}}_\mathrm{s} = 1/2(\underline{\mathbf{b}}_1\underline{\mathbf{b}}_2 + \underline{\mathbf{b}}_2\underline{\mathbf{b}}_1)$ denotes the shear direction unit tensor. The prime $\circ'$ denotes the derivative of a function with respect to its single argument. For simplicity an isotropic elastic matrix $\underset{\approx}{\mathbf{S}} = 2\mu\underset{\approx}{\mathbf{I}}^\mathrm{s} + \lambda\underset{\sim\sim}{\mathbf{II}}$ is assumed with μ and λ being Lamé's constants. With material laws Eqs. (33) to (35) the stresses are

$$\begin{aligned}
\underset{\sim}{\mathbf{\Sigma}} &= 2\mu\left[\left(1 - f + F^{Ee}(f)\right)U_\mathrm{s}' - F^{Ee}(f)\chi_\mathrm{s}\right]\underset{\sim}{\mathbf{N}}_\mathrm{s} \\
\underline{\mathbf{s}} &= 2\mu\left[\left(F^{ee}(f) + F^{Ee}(f)\right)U_\mathrm{s}' - F^{ee}(f)\chi_\mathrm{s}\right]\underset{\sim}{\mathbf{N}}_\mathrm{s} \\
\underline{\underline{\mathbf{M}}} &= 2\mu R^2 F^K(f)\chi_\mathrm{s}'\underset{\sim}{\mathbf{N}}_\mathrm{s}\underline{\mathbf{b}}_2\,.
\end{aligned} \tag{46}$$

Inserting these stresses into balance equations (12) and (13) gives a system of linear ordinary differential equations for the unknown functions $U_\mathrm{s}\left(X_2\right)$ and $\chi_\mathrm{s}\left(X_2\right)$. In addition to the classical boundary displacement conditions $U_\mathrm{s}\left(0\right) = 0$ and $U_\mathrm{s}\left(h\right) = \hat{U}_\mathrm{s}$, boundary conditions for the higher order deformations have to be specified. Here, so-called "micro-clamped" boundary conditions $\chi_\mathrm{s}\left(0\right) = \chi_\mathrm{s}\left(h\right) = 0$ are prescribed in order to address size effects. Then the solution may be found by standard mathematical methods as

$$\begin{aligned}
\chi_\mathrm{s}\left(X_2\right) &= \frac{\hat{U}_\mathrm{s}}{h}\cdot\left(1 + \frac{F^{Ee}}{F^{ee}}\right)\cdot\frac{\cosh\frac{h}{2\hat{R}_\mathrm{s}} - \cosh\frac{h-2X_2}{2\hat{R}_\mathrm{s}}}{\cosh\frac{h}{2\hat{R}_\mathrm{s}} - \frac{(F^{ee}+F^{Ee})^2}{(1-f+F^{ee}+2F^{Ee})F^{ee}}\,\frac{\sinh(h/(2\hat{R}_\mathrm{s}))}{h/(2\hat{R}_\mathrm{s})}} \\
U_\mathrm{s}\left(X_2\right) &= \frac{\hat{U}_\mathrm{s}}{h}\left[X_2 + \hat{R}_\mathrm{s}\cdot\frac{\cosh\frac{h-2X_2}{2\hat{R}_\mathrm{s}} - \frac{h-2X_2}{\hat{R}_\mathrm{s}}\sinh\frac{h}{2\hat{R}_\mathrm{s}}}{\frac{(1-f+F^{ee}+2F^{Ee})F^{ee}}{(F^{ee}+F^{Ee})^2}\cosh\frac{h}{2\hat{R}_\mathrm{s}} - \frac{\sinh(h/(2\hat{R}_\mathrm{s}))}{h/(2\hat{R}_\mathrm{s})}}\right].
\end{aligned} \tag{47}$$

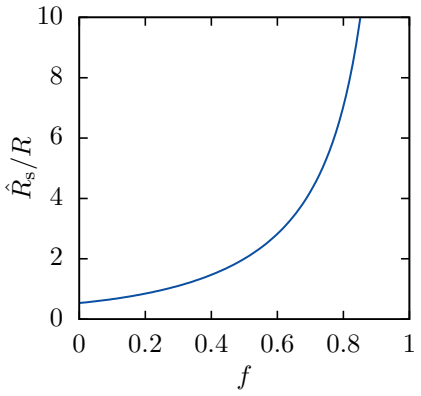

Figure 4: Effect of void volume fraction on characteristic length (spherical voids)

Therein, the abbreviation

$$\hat{R}_s = R\sqrt{\frac{F^K(f)\,[1-f+F^{ee}(f)+2F^{Ee}(f)]}{(1-f)\,F^{ee}(f)-\left(F^{Ee}(f)\right)^2}} \tag{48}$$

was introduced for the length that arises mathematically from the characteristic equation of the system of ordinary differential equations for simple shear. The plot against the void volume fraction f for spherical voids in Figure 4 shows that for low f the value $\hat{R}_s$ lies in the range of R but increases significantly with further increasing f. In general, the value R is to be interpreted as half mean void distance.

The distribution of the shear microdeformation χ_s for simple shearing is plotted in Figure 5 for different ratios of height h of the specimen and material length R. It shows that for small specimens χ_s is non-homogeneous over the whole thickness whereas for large specimens $h/R = 50$ a region of constant deformations is formed in the center and the inhomogeneous deformations are limited to boundary layers of finite size at the surfaces. In contrast, the total stress $\underset{\sim}{\boldsymbol{\Sigma}} + \underset{\sim}{\mathbf{s}}$ is constant over the whole thickness due to balance of momentum Eq. (12). Inserting the solution Eqs. (47) back into material laws Eq. (46) yields a macroscopic shear stress of

$$\tau_s = \left(\underset{\sim}{\boldsymbol{\Sigma}} + \underset{\sim}{\mathbf{s}}\right) : \underset{\sim}{\mathbf{N}}_s = \frac{\mu \hat{U}_s}{h} \cdot \frac{1-f-\frac{\left(F^{Ee}\right)^2}{F^{ee}}}{1-\frac{(F^{ee}+F^{Ee})^2}{(1-f+F^{ee}+2F^{Ee})F^{ee}}\frac{\tanh(h/(2\hat{R}_s))}{h/(2\hat{R}_s)}} \,. \tag{49}$$

The result for a classical Cauchy continuum can be easily identified by the limit case $h/\hat{R}_s \to \infty$ as $\tau_s^{\infty} = \left[1-f-\left(F^{Ee}\right)^2/F^{ee}\right]\mu\hat{U}_s/h$. For finite values of the ratio of height h and characteristic length $\hat{R}_s$, or equivalently mean half void distance R, the shear stress is plotted in Figure 6 for given mean shear strain $\hat{U}_s/h$. Due to the linearity of the material behavior the plotted ratio corresponds directly to the relative stiffness of the specimen. The graph shows the transition between the two limit cases $h/R \to \infty$ and $h/R \to 0$ (the latter being of course a purely mathematical solution conflicting with the assumptions of the homogenization). For low void volume fractions of $f = 0.001$ to $f = 0.1$ a moderate stiffening with decreasing strip thickness h is predicted. Although being weaker in magnitude, the size-effect does not vanish completely for $f = 0$. Such artificial size-effects are known from constrained higher order theories [12, 31]. It remains open to clarify whether this effect is a relict of the approximate solution (14) or whether it is attributed to the employed homogenisation theory itself. For higher void volume fractions $f > 0.1$ the size effect becomes more distinct. Furthermore, it is found that the transition region on the h/R axis in Figure 6 is the wider, the higher f is. So for $f \geq 0.5$ the size

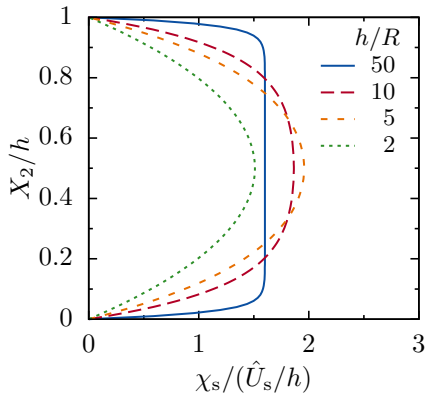

Figure 5: Microdeformation for $f = 0.30$ (spherical voids)

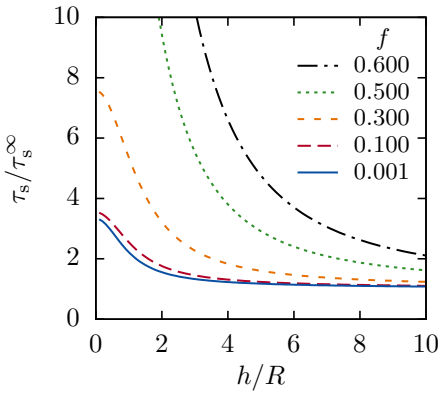

Figure 6: Shear stress for prescribed mean shear $\hat{U}_s/h$ relative to classical theory (spherical voids)

effect does not saturate the strip height reaches a value $h \approx 10R$. This behavior is plausible due to the stronger interaction of the voids. Mathematically, it is is attributed to the increase of the characteristic length $\hat{R}_s$ relative to the mean void half distance R with increasing void volume fraction f as shown already in Figure 4.

The used unit cell with void (Figure 1) raises the suspicion that the obtained elastic micromorphic law might be suitable to describe the size effects of elastic closed-cell foams. Figure 6 shows that the derived theory predicts for intermediate void volume fractions f up to 0.5 a shear stiffness of small specimens $h = (2 \dots 4)R$ of a factor τ_s/τ_s^∞ of 1.5 to 4 compared to large specimens. This amount of stiffening lies indeed in the range of experimental results compiled by Lakes [2, 3]. Waseem et al. [32] performed bending tests with foam-like structures (with drilled and regularly arranged holes) and observed, in agreement with the predictions of the present model, indeed an increasing size-effect for increasing void volume fractions.

In addition to the amount of stiffening that is attainable with small specimens, the second important question is whether the particular specimen sizes can be predicted at which the size effect initiates, i.e. whether the location of transition region on the abscissa between the two limit cases in Figure 6 is realistic. Finite element simulations of simple shearing of elastic foams with discretely resolved microstructure were performed by Tekoğlu and co-workers [4, 6] and Jänicke et al. [33]. Tekoğlu and co-workers performed simulations with random Voronoi-tessellated foams modeled by beam elements. They published average and lower and upper bound values of the obtained macroscopic stiffness that are plotted in Figure 6. For such a random microstructure, the length R is interpreted as mean value computed as radius of the mean area-equivalent cell. Jänicke et al. [33] investigated perfectly regular honeycomb structures and slightly disturbed modifications thereof with more accurate 2D continuum elements on the microstructure level. Unfortunately, the latter authors investigated only specimen sizes where the size effect is still relatively weak.

Both research groups used 2D models. For this reason their results are compared in Figure 7 with the analytical predictions (49) of the present homogenized model, but now with the coefficients for circular voids from section 4. Solution (49) remains valid then but coefficients F^{ee}, F^{Ee} and F^K have to be replaced by the 2D values (40). Figure 7 shows that the present homogenized model with $f = 0.4 \dots 0.6$ matches the simulation results for the discrete microstructure from literature quite well. However, it has to be remarked that the microstructure in the latter simulations corresponds to void volume fractions of about 0.9. Thus, in this regime of f the present model apparently overestimates the size effect. This overestimation is related to the steep increase of the characteristic length $\hat{R}_s$ in this regime (see Figure 4). The steep increase comes again from the coefficient functions $F^{ee}(f)$ and $F^{ee}(f)$ in the

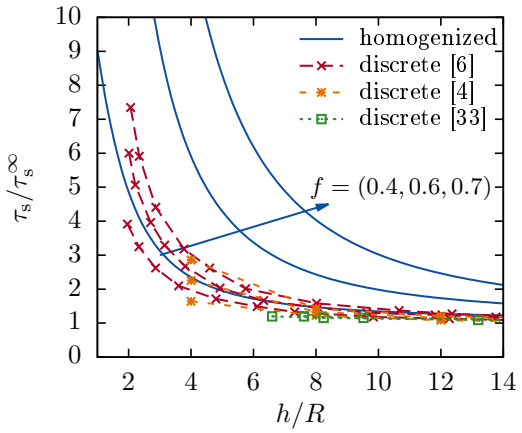

Figure 7: Size-effect in simple shearing predicted by the present homogenized model with circular voids compared to simulations with discretely resolved microstructure [4, 6, 33]

denominator of definition (48) of $\hat{R}_s$. The functions $F^{ee}(f)$ and $F^{ee}(f)$ derive from the polynomial approximation of the local displacement field and is possibly not accurate enough for high void volume fractions $f \gtrsim 0.6$. And possibly for that large f also the exact topology of a foam, which is not covered by the present model, has an effect on the size effect. From this point of view a slight calibration of the mean cell radius R of the present model may be reasonable to match particular (numerical or real) experiments better.

In all but one of the just mentioned numerical and experimental studies from literature Cosserat theory (a special case of micromorphic theory) is employed to model the observed size-effects. Possibly Cosserat theory was chosen due to the considerably lower number of independent material parameters compared to fully micromorphic theory since the constitutive parameters were determined in all these studies by a fitting procedure. However, Lakes points already out that Cosserat theory is unable to describe some of the observed size effects like the dispersion of longitudinal waves. For this reason Lakes proposes to use fully micromorphic theories as perspective. In the present contribution a homogenization for a fully micromorphic theory was performed so that the derived model is able to describe the lacking effects. Remarkably, although allowed in the ansatz Eq. (14) (due to the unrestricted cubic polynomial coefficient tensor $\underset{\approx}{\mathbf{D}}$) the Cosserat terms drop out due to the regular geometry of the RVE and a microstrain theory is obtained.

5.2 Damage Model for Quasi-brittle Materials

Quasi-brittle materials like ceramics or concrete soften due to initiation and propagation of microcracks. Typically, these microcracks initiate at voids or inclusions. Mühlich et al. [31] formulated a corresponding damage model by assuming that the damaged spherical layer of thickness Δa can be considered as effective void growth as sketched in Figure 8. Thus, they introduce the effective void volume fraction

$$f^{\text{eff}} = \left(\frac{R_{\text{void}} + \Delta a}{R} \right)^3 . \tag{50}$$

after some amount of crack growth Δa as internal variable. This approach is adopted here to derive a micromorphic damage mechanics model based on the presented homogenization. It is assumed that no residual strains appear during quasi-brittle failure so that the damaged zone stores no strain energy anymore. Thus, the Helmholtz energy as state function is obtained by inserting f^{eff} instead of f into Eq. (31). Furthermore, an evolution equation for f^{eff} has to be formulated. For this purpose the dissipation $\mathcal{D}$ associated with microcrack growth is investigated. It is assumed that a number n of microcracks

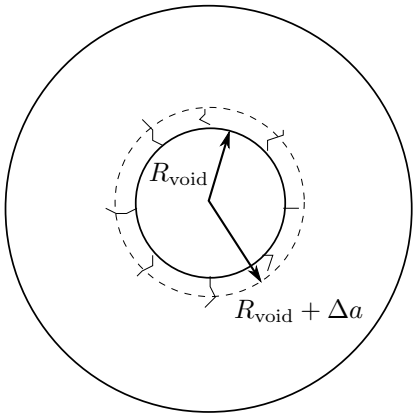

Figure 8: Increase of effective void volume fraction due to propagation of microcracks

propagate whose crack fronts remain circular. Thus, for a fracture toughness of the matrix material Γ_0 (which may depend on Δa), the dissipation during ongoing microcrack growth is

$$\mathcal{D} = n\Gamma_0 2\pi(R_{\text{void}} + \Delta a)\Delta\dot{a}\,. \tag{51}$$

By means of Eq. (50) this expression can be rearranged to

$$\mathcal{D} = \frac{2\pi n R^2 \Gamma_0}{3\sqrt[3]{f^{\text{eff}}}}\dot{f}^{\text{eff}}\,. \tag{52}$$

Macroscopically, the Clausius-Duhem inequality $\mathcal{D} = Z\dot{f}^{\text{eff}}V \geq 0$ has to hold with $V = 4\pi/3R^3$ and $Z = -\Psi_{,f^{\text{eff}}}$ being the driving force (or energy release rate) of $\dot{f}^{\text{eff}}$. Thus, for ongoing microcrack growth $\dot{f}^{\text{eff}} \geq 0$, Eq. (52) has to be equal to $Z\dot{f}^{\text{eff}}V$. Otherwise, there is no growth of microcracks, i.e. $\dot{f}^{\text{eff}} = 0$. This behavior can be expressed in terms of a damage function

$$\Phi = Z - \gamma(f^{\text{eff}}) \tag{53}$$

with material resistance[3]

$$\gamma(f^{\text{eff}}) = \frac{n\Gamma_0}{2R\sqrt[3]{f^{\text{eff}}}} \tag{54}$$

and the corresponding loading-unloading conditions

$$\Phi \leq 0, \qquad \dot{f}^{\text{eff}} \geq 0, \qquad \Phi\dot{f}^{\text{eff}} = 0\,. \tag{55}$$

For the particular state potential Eq. (31) the driving force is

$$Z = \frac{1}{2}\underset{\sim}{\mathbf{E}} : \underset{\approx}{\mathbf{S}} : \underset{\sim}{\mathbf{E}} - \frac{R^2}{2}\left(F^K\right)'\left(\underset{\sim}{\mathbf{K}}^{\mathrm{T}} : \underset{\approx}{\mathbf{S}} : \underset{\sim}{\mathbf{K}}\right) : \underset{\sim}{\mathbf{I}} - \frac{1}{2}\left(F^{ee}\right)'\underset{\sim}{\mathbf{e}} : \underset{\approx}{\mathbf{S}} : \underset{\sim}{\mathbf{e}} - \left(F^{Ee}\right)'\underset{\sim}{\mathbf{E}} : \underset{\approx}{\mathbf{S}} : \underset{\sim}{\mathbf{e}}\,. \tag{56}$$

Again, the prime $\circ'$ denotes the derivative of a function with respect to its single argument, i.e. here with respect to f^{eff}. Note firstly that in Eq. (56) the driving force Z remains finite at $f^{\text{eff}} = 1$ for given deformations $\underset{\sim}{\mathbf{E}}$, $\underset{\sim}{\mathbf{K}}$ and $\underset{\sim}{\mathbf{e}}$. Secondly, it can be found that in absence of higher order deformations $\underset{\sim}{\mathbf{K}} = 0$ and $\underset{\sim}{\mathbf{e}} = 0$, the proposed model reduces to the Kachanov effective stress type isotropic damage model

[3] For the model with circular voids from section 4 analogous considerations lead to $\gamma(f^{\text{eff}}) = n\Gamma_0/\left(\pi R\sqrt{f^{\text{eff}}}\right)$.

with $(1-f^{\mathrm{eff}})$ as prefactor of the strain energy density $1/2\underset{\sim}{\mathbf{E}} : \underset{\approx}{\mathbf{S}} : \underset{\sim}{\mathbf{E}}$ of the compact matrix material, compare e.g. [34]. In the context of such models the internal variable f^{eff} is denominated just as damage variable. Some extensions of effective stress damage models to implicit gradient enriched non-local continuum theories (it is recalled that according to Forest [16] such formulations fit in the framework of generalized micromorphic media) have been proposed in the literature [e.g. 35–39]. Therein, higher order terms that contain the intrinsic length are included typically linearly and reversibly (corresponding to $\underset{\approx}{\underset{\sim}{\mathbf{M}}} = c\underset{\approx}{\underset{\sim}{\mathbf{K}}}$ in present notation with a constant c) the problems mentioned in section 1. The model proposed in the present study overcomes this problems as all material parameters are determined by a homogenization procedure. So despite the finite driving force, all stress quantities $\underset{\sim}{\boldsymbol{\Sigma}}$, $\underset{\sim}{\mathbf{s}}$ and $\underset{\approx}{\underset{\sim}{\mathbf{M}}}$ vanish with $f^{\mathrm{eff}} \to 1$ as the corresponding prefactors do, Figure 2. Thus, a free surface , i.e. with trivial natural boundary conditions $\left(\underset{\sim}{\boldsymbol{\Sigma}} + \underset{\sim}{\mathbf{s}}\right) \cdot \underline{\mathbf{n}} = 0$ and $\underset{\approx}{\underset{\sim}{\mathbf{M}}} \cdot \underline{\mathbf{n}} = 0$ associated to the equilibrium conditions (12)–(13), arises naturally in the fully damaged state $f^{\mathrm{eff}} = 1$.

6 Summary and Outlook

In the present paper the unconstrained micromorphic constitutive law of an elastic porous medium is obtained by homogenization. For this purpose the minimal boundary conditions concept is applied so that the model is consistent with Germain's homogenization concept for micromorphic media. A closed form solution of the resulting boundary-value problem on the microscale is derived by Ritz' method for arbitrarily anisotropic (but homogeneous) linear elastic properties of the matrix material. Although not precluded from the ansatz, the Cosserat (micropolar) terms cancel out and a microstrain theory is obtained. The theory is applied to the simple shearing problem and shows a stiffening effect when the thickness of the layer becomes comparable to the distance of the voids, an effect that is well-known from experiments with closed-cell foams and from simulations with discretely resolved microstructure. It is found that the size effect is stronger, the higher the void volume fraction is, a behavior that is plausible since the void interaction becomes more dominant for higher void volume fractions.

Based on the micromorphic model for elastic porous media, a damage model for quasi-brittle materials is proposed accounting for micro-crack initiation and growth by introducing an effective void volume fraction. It turns out that under homogeneous loading conditions the presented model reduces to an Kachanov-Lemaitre effective stress type model with isotropic damage. Models of this type have been extended heuristically to implicit gradient-enriched formulations already in literature. Such models fit also into the (generalized) framework of micromorphic continua. In contrast to these heuristic approaches, in the presented model all material parameters have a clear physical meaning as well as the gradient terms and the conjugate higher order stresses have. Correspondingly, the formation of free surfaces with vanishing stresses and higher-order stresses when reaching the fully damaged state is, in contrast to heuristic gradient models, an natural outcome of the derived model.

It remains open to investigate the macroscopic localization and fracture behavior predicted by the presented model in detail and compare it with corresponding experimental results. Also the predicted size effect in the elastic regime requires verification by experimental data. The derived model is obtained by an approximate solution by means of Ritz' method. The solution can be further refined by incorporating higher order polynomial ansatz functions or ansatz functions that eventually contain known exact solutions for some special cases like e.g. Lamé's solution of a hollow sphere under hydrostatic loading. Although surely expansive in the particular implementation, the procedure for refining the solution is straight-forward by means of the employed homogenization method. It will be interesting to see whether such a refined solution eliminates the (weak) artificial size effect that is predicted by the present model for a vanishing void volume fraction.

Acknowledgments

The authors thank Rostyslav Skrypnyk for proofreading the manuscript.

References

[1] Eringen, A.C., Suhubi, E.S.. Nonlinear theory of simple micro-elastic solids–i. Int J Eng Sci 1964;2(2):189–203.

[2] Lakes, R.S.. Size effects and micromechanics of a porous solid. J Mater Sci 1983;18(9):2572–2580.

[3] Lakes, R.S.. Experimental microelasticity of two porous solids. Int J Solids Struct 1986;22(1):55–63.

[4] Tekoğlu, C., Gibson, L., Pardoen, T., Onck, P.. Size effects in foams: Experiments and modeling. Prog Mater Sci 2011;56(2):109–138.

[5] Branke, D.. Homogenisierungsmethode für den Übergang vom CAUCHY- zum COSSERAT-Kontinuum. Dissertation; TU Dresden; 2012.

[6] Tekoğlu, C., Onck, P.R.. Size effects in two-dimensional Voronoi foams: A comparison between generalized continua and discrete models. J Mech Phys Solids 2008;56(12):3541–3564.

[7] de Borst, R., Sluys, L., Muhlhaus, H.B., Pamin, J.. Fundamental issues in finite element analyses of localization of deformation. Eng Computation 1993;10(2):99–121.

[8] Forest, S., Sab, K.. Cosserat overall modeling of heterogeneous materials. Mech Res Commun 1998;25(4):449–454.

[9] Jänicke, R., Diebels, S., Sehlhorst, H.G., Düster, A.. Two-scale modelling of micromorphic continua. Continuum Mech Therm 2009;21(4):297–315.

[10] Jänicke, R., Steeb, H.. Wave propagation in periodic microstructures by homogenisation of extended continua. Comp Mater Sci 2012;52(1):209–211.

[11] Zybell, L., Mühlich, U., Kuna, M.. Constitutive equations for porous plane-strain gradient elasticity obtained by homogenization. Arch Appl Mech 2009;79(4):359–375.

[12] Gologanu, M., Leblond, J., Perrin, G., Devaux, J.. Recent extensions of Gurson's model for porous ductile metals. In: Suquet, P., editor. Continuum micromechanics. No. 377 in Cism Courses And Lectures: International Centre For Mechanical Sciences Series; New York: Springer-Verlag; 1997, p. 61–130.

[13] Bigoni, D., Drugan, W.J.. Analytical derivation of Cosserat moduli via homogenization of heterogeneous elastic materials. J Appl Mech 2006;74(4):741–753.

[14] Yuan, X., Tomita, Y., Andou, T.. A micromechanical approach of nonlocal modeling for media with periodic microstructures. Mech Res Commun 2008;35(1–2):126–133.

[15] Li, J.. Establishment of strain gradient constitutive relations by homogenization. C R Mécanique 2011;339(4):235–244.

[16] Forest, S.. Micromorphic approach for gradient elasticity, viscoplasticity, and damage. J Eng Mech 2009;135(3):117–131.

[17] Forest, S., Ammar, K., Appolaire, B.. Micromorphic vs. phase-field approaches for gradient viscoplasticity and phase transformations. In: Markert, B., editor. Advances in Extended and Multifield Theories for Continua; vol. 59 of Lecture Notes in Applied and Computational Mechanics. Springer Berlin / Heidelberg; 2011, p. 69–88.

[18] Hütter, G., Linse, T., Mühlich, U., Kuna, M.. Simulation of ductile crack initiation and propagation by means of a non-local GTN-model under small-scale yielding. Int J Solids Struct 2013;50:662–671.

[19] Forest, S., Sievert, R.. Nonlinear microstrain theories. Int J Solids Struct 2006;43(24):7224–7245.

[20] Germain, P.. The method of virtual power in continuum mechanics. part 2: Microstructure. Siam J Appl Math 1973;25(3):556–575.

[21] Forest, S.. Homogenization methods and the mechanics of generalized continua - part 2. Theoretical and Applied Mechanics 2002;28-29:113–143.

[22] Forest, S., Trinh, D.K.. Generalized continua and non-homogeneous boundary conditions in homogenisation methods. Z Angew Math Mech 2011;91(2):90–109.

[23] Jänicke, R., Steeb, H.. Minimal loading conditions for higher order numerical homogenisation schemes. Arch Appl Mech 2012;82(8):1075–1088.

[24] Forest, S.. Mechanics of Cosserat media – an introduction. Ecole des Mines de Paris; 2005.

[25] Jänicke, R.. Micromorphic media: Interpretation by homogenisation. Dissertation; Universität des Saarlandes; Saarbrücken; 2010.

[26] Mühlich, U., Zybell, L., Kuna, M.. Estimation of material properties for linear elastic strain gradient effective media. Eur J Mech A-Solid 2012;31(1):117–130.

[27] Aifantis, E.C.. The physics of plastic deformation. Int J Plasticity 1987;3(3):211–247.

[28] Forest, S.. Questioning size effects as predicted by strain gradient plasticity. Journal of the Mechanical Behavior of Materials 2013;22:101–110.

[29] Aifantis, K.E., Willis, J.R.. The role of interfaces in enhancing the yield strength of composites and polycrystals. J Mech Phys Solids 2005;53(5):1047–1070.

[30] Mazière, M., Forest, S.. Strain gradient plasticity modeling and finite element simulation of Lüders band formation and propagation. Continuum Mech Therm 2013;doi:10.1007/s00161-013-0331-8.

[31] Mühlich, U., Zybell, L., Hütter, G., Kuna, M.. A first-order strain gradient damage model for simulating quasi-brittle failure in porous elastic solids. Arch Appl Mech 2013;83:955–967.

[32] Waseem, A., Beveridge, A., Wheel, M., Nash, D.. The influence of void size on the micropolar constitutive properties of model heterogeneous materials. Eur J Mech A-Solid 2013;40:148–157.

[33] Jänicke, R., Sehlhorst, H.G., Duster, A., Diebels, S.. Micromorphic two-scale modelling of periodic grid structures. Int J Multiscale Com 2013;11(2):161–176.

[34] Lemaitre, J., Chaboche, J.L.. Mechanics of solid materials. Cambridge University Press; 1994.

[35] Geers, M.G.D., de Borst, R., Brekelmans, W.A.M., Peerlings, R.H.J.. Strain-based transient-gradient damage model for failure analyses. Comput Method Appl M 1998;160(1–2):133–153.

[36] Geers, M.G.D., Peerlings, R.H.J., Brekelmans, W.A.M., de Borst, R.. Phenomenological nonlocal approaches based on implicit gradient-enhanced damage. Acta Mech 2000;144(1):1–15.

[37] Dimitrijevic, B.J., Hackl, K.. A method for gradient enhancement of continuum damage models. Tech Mech 2008;28(1):43–52.

[38] Jirásek, M.. Nonlocal models for damage and fracture: Comparison of approaches. Int J Solids Struct 1998;35(31–32):4133–4145.

[39] Simone, A., Wells, G.N., Sluys, L.J.. From continuous to discontinuous failure in a gradient-enhanced continuum damage model. Comput Method Appl M 2003;192(41–42):4581–4607.